Generalisation for thunderstorm downburst wind design spectra

Song, Jing; Martinez-Vazquez, Pedro; Skalomenos, Konstantinos

Document Version
Peer reviewed version

Link to publication on Research at Birmingham portal

Generalisation for thunderstorm downburst wind design spectra

*Jing Song[1], Pedro Martinez-Vazquez[2], Konstantinos A. Skalomenos[3]

[1], [2], [3] *Department of Civil Engineering, University of Birmingham, Birmingham, B15 2TT, United Kingdom*
[1] *jxs1223@bham.ac.uk*

ABSTRACT

In recent years, design spectra tailored to thunderstorm downbursts, revealed as a promising tool to evaluate the dynamic response on structures. The design tool merges methods commonly used in earthquake-resisting design with aerodynamic characteristics of thunderstorm downbursts and their interaction with structures. This initial step is now refined through the generalisation of the spectra, via non-linear regression modelling. The result is a multi-factorial polynomial equation that captures the influence of controlling parameters that determine the corresponding wind-structure interaction. The effectiveness of the simulated design spectra was validated through comparison with results obtained for the CAARC benchmark building when using the non-synthetic design spectra. To conclude that design spectra simulated in this way, could be used to run the standard modal analysis with the help of commercial software. The proposed model can therefore be regarded as an alternative to estimate the dynamic response on structures subjected to transient winds.

1. INTRODUCTION

The severe damages induced to infrastructure by transient winds has generated multiple studies to better understand structural performance under the action of thunderstorm downbursts. A portion of those studies identified microbursts going through buildings blocks, via full-scale measurements (Lombardo et al., 2018). Those results also expanded through numerical and experimental simulations (Asano et al., 2019; Haines & Taylor, 2018; Jesson, Sterling, Letchford, & Baker, 2015; Jesson, Sterling, Letchford, & Haines, 2015) including some microburst field simulations (Chen & Letchford, 2004;

---

[1] PhD Candidate, E-mail: jxs1223@bham.ac.uk
[2] Professor
[3] Professor

Solari et al., 2017). Those valuable contributions have therefore enhanced our knowledge of the relevant structural design and wind loads (Solari, 2020). However, further work is needed in this field, due to the fact that current design standards do not fully address the effects of wind actions induced by the downburst outflows on structures.

Based on the early work by Davenport's chain for synoptic wind (Dyrbye & Hansen, 1997), Kareem et al. (2019) put forward a generalised wind loading chain framework combined with evolutionary power spectral density and wavelet transform methods, to address the relationship of wind-force-response in the time-frequency domain. Further work by Peng et al. (2018), focused on the effects of the time-varying coherence of the non-stationary wind on the dynamic response on structures, which pose some differences with the time-invariant coherence function used for various studies by Chen and Letchford (2004), and Solari (2016). Le and Caracoglia (2017) also formulated a numerical model to investigate the dynamic response of a tall building considering the buffeting effects induced by transverse wind.

In this paper, we revisit the basic formulation that gave place to thunderstorm downburst wind design spectra (TWDS), as a basis for their generalisation.

2. THE ORIGINAL FORMULATION TO GENERATE THUNDERSTORM DOWNBURST WIND DESIGN SPECTRA

This section outlines the algorithm developed by Song et al. (2021) for generating TWDS. That technique requires knowledge on mechanical and aerodynamical admittance mechanisms that translate wind loading acting on prismatic buildings into their structural response. The method takes to vibrate Multi-degree of Freedom (MDOF) systems converted into their Single degree of Freedom (SDOF) equivalent oscillators, to determine their dynamic response. This method initially captures the first mode of vibration of the SDOF structures, to then unfold the multi-modal response of MDOF buildings, via classical modal spectral analyses.

2.1 Mathematical framework

Previous researches have confirmed numerous times that the *rms* of the fluctuating output response can be obtained by the integration of the spectral density of the response in the frequency domain. Those concepts have been widely used in earthquake engineering applications, while more recently for wind-resisting design. According to the latter, the physical relationship between the input and output (response) acceleration can be established with Eq. (1) and (2). In that formulation, the force factor is purely induced by fluctuating turbulence i.e., $f' = 0.5c_D\rho A(2\overline{U}u' + u'^2)$; where it follows that the second-order term of the fluctuating turbulence, u'^2, can be approximated by $\sigma_u u'$ i.e., $2\overline{U}u' + u'^2 = (2\overline{U} + u')u' \approx (2\overline{U} + \sigma_u)\sigma_u \tilde{u}' \approx (2\overline{U} + I_u\overline{U})I_u\overline{U}\tilde{u}'$. The formulation also uses the normalised cross spectra proposed by Davenport (1977) (see Eq. (4)) to quantify the spatial correlation of wind gusts acting on area-like members. It follows that, by combining the spectra of input acceleration given in Eq. (2) with the cross spectra of the horizontal turbulence component given in Eq. (4), the cross-spectrum of the input acceleration can be obtained, see Eq. (5).

The integration of Eq. (5) across the area exposed to wind flow, contributes to the power spectral density of the generalised input acceleration, $S_{cu}(z_i, z_j, n)$, given in Eq. (6). This provides the acceleration inputted to a system, therefore the variance of the overall spectral response can be obtained by passing the signal through the transfer function. The design spectra of the output acceleration (see Eq. (10)) can finally be derived with the square root of the sum of the background component (see Eq. (7)) and the resonant component (see Eq. (8)). Table 1 summarises the mathematical framework proposed to calculate TWDS.

Table 1. Summarised processes for thunderstorm downburst wind design spectra.

	Input data	Equations	
		Stage 1: Spectrum of Input Acceleration	
S_F	Force spectra	$S_F(z,n) = q^2(z)S_{\tilde{u}'}(z,n)$	(1)
S_A	Spectrum of input acceleration	$S_A(z,n) = \left(\dfrac{q(z)}{m}\right)^2 S_{\tilde{u}'}(z,n)$	(2)
$S_{\tilde{u}'}$	Wind velocity power spectrum for reduced horizontal fluctuating velocity component $\tilde{u}'$	$nS_{\tilde{u}'}(z,n) = \dfrac{18f}{[1+27f]^{5/3}}$	
m	Mass of the structure excited by the wind force	$f = nz/\bar{U}_{max}(z)$	
n	The frequency of gust wind		
z	Height above the ground		
q	Force factor		
m_1	First modal mass per unit height	$m_1 = \displaystyle\int_0^H m_l(z)\phi_1^2(z)dz$	
m_l	Structural mass per unit height		
ϕ_1	First modal shape	$\phi_1(z) = (^z/_H)^\psi$	
ψ	Modal shape factor		
H	Structural height		
c_D	Drag coefficient	$q(z) = c_D(z)\rho A(z)\bar{U}_{max}^2(z)[1 + 0.5\bar{I}_u(z)]\bar{I}_u(z)$	(3)
ρ	Air density		
$\bar{U}_{max}$	Maximum slowly varying mean velocity		
$\bar{I}_u$	Slowly varying mean turbulence intensity		
A	Area of the structures exposed to wind		
		Stage 2: Cross-Spectrum of Input Acceleration	
χ	Aerodynamic admittance	$\chi(z,n)$	(4)
C_y, C_z	Decay constant in horizontal y and vertical z direction, taken as 10	$= exp\left\{-\dfrac{n}{1/2[\bar{U}_{max}(z_i) + \bar{U}_{max}(z_j)]}\sqrt{(C_y\Delta_y)^2 + (C_z\Delta_z)^2}\right\}$	
Δ_y, Δ_z	The horizontal and vertical distances between two points, $i, j,$ located at coordinates $\{y_i, z_i\}$ and $\{y_j, z_j\}$ respectively		
$S_{A_{ij}}$	Cross spectrum of input acceleration	$S_{A_{ij}}(z_i, z_j, n)$ $= \dfrac{1}{m^2}q(z_i)q(z_j)\sqrt{S_{\tilde{u}'}(z_i,n)S_{\tilde{u}'}(z_j,n)}\dfrac{1}{A^2}\chi(z_i,z_j,n)$	(5)
S_{cu}	Generalised cross-spectrum of input acceleration	$S_{cu}(z_i, z_j, n) = \iint_A \phi(z_i)\phi(z_j)S_{A_{ij}}(z_i, z_j, n)dy_i dy_j dz_i dz_j$	(6)
		Stage 3: Thunderstorm downburst wind design spectrum	

$\sigma_{a,b}$	Background dynamic response	$\sigma_{a,b}^2 = \displaystyle\int_0^\infty S_{cu}(z_i, z_j, n)dn$	(7)
$\sigma_{a,r}$	Resonant dynamic response	$\sigma_{a,r}^2 = S_{cu}(z_i, z_j, n_0)\displaystyle\int_0^\infty |J(n)|^2 dn \cong \dfrac{\pi n_0 S_{cu}(z_i, z_j, n_0)}{4\xi}$	(8)
$J(n)$	Transfer function	$J(n) = \dfrac{1}{\sqrt{[1 - (n/n_0)^2]^2 + 4\xi^2 (n/n_0)^2}}$	
n_0	The natural frequency of structures		
ξ	Damping ratio		
σ_a	Dynamic response	$\sigma_a^2 = \displaystyle\int_0^\infty |J(n)|^2 S_{cu}(z_i, z_j, n)dn$	(9)
S_a	Thunderstorm downburst wind design spectrum	$S_a = \sqrt{\sigma_a^2} = \sqrt{\sigma_{a,b}^2 + \sigma_{a,r}^2}$	(10)

2.2 Investigation of input parameters

The multi-dimensional nature of TWDS of the output acceleration can be represented by Eq. (11). The input parameters include the maximum slowly varying mean velocity at reference height ($\bar{U}_{max,r}$), the width of the building (W), the chord length (L), the height of the building (H), the height for the peak slowly varying mean velocity ($\bar{U}_{peak}$), damping ratio (ξ), structural mass (m_v), drag coefficient (C_D), terrain type, and modal shape factor (ψ).

$$S_a = f(\bar{U}_{max,r}, W, L, H, z_{\bar{U}_{peak}}, \xi, m_v, C_D, terrain, \psi) \qquad (11)$$

Fig. 1 outlines the effects of the identified input parameters on the TWDS. In this formulation, the reference maximum slowly varying mean velocity is a dominant input, as its magnitude covers a large range. For example, when $\bar{U}_{max,r}$ equals 50 m/s and 70 m/s, respectively, the output structural acceleration S_a passes from 0.292 m/s^2 to 0.652 m/s^2 for a building whose natural frequency is of 0.1 s. The influence of the building width can be illustrated when observing that S_a slightly descends from 0.066 m/s^2 to 0.045 m/s^2 when W passes from 10 m to 50 m, the 32% decrease, for the same fundamental frequency of 0.1 s. Fig. 1(c) and Fig. 1(d) show the influence of the varying height (from 20 m to 200 m) and chord width (from 8 m to 40 m) on the output acceleration. Is also worth to note that, without having evidence that demonstrates the opposite the cross-correlation of input parameters is negligible.
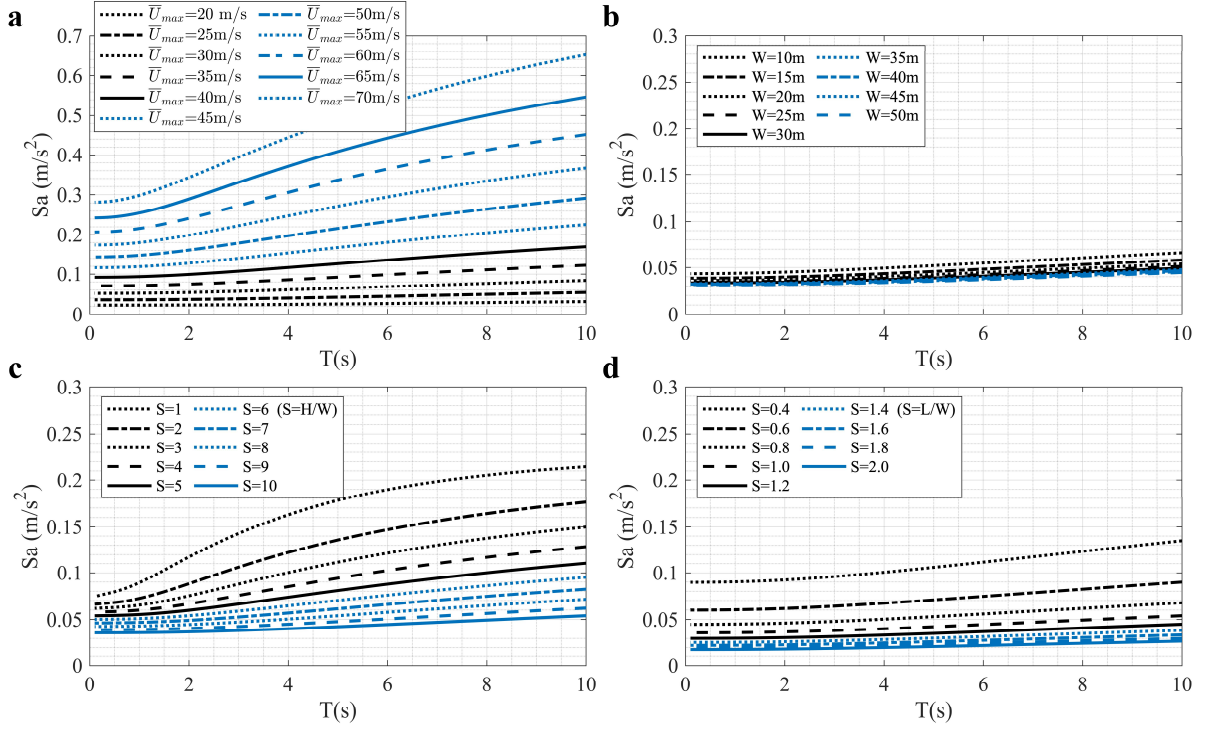
Fig. 1. TWDS of output acceleration with varying input parameters (Default values: $\overline{U}_{max,10}$=25 m/s, W=20 m, H=200 m, L=20 m, ξ=0.025, $z_{\overline{U}_{peak}}$=50 m, Terrain exposure B, m_v=384 kg/m³, c_d=1 and ψ=1.5).

3. THREE-DIMENSIONAL NON-LINEAR REGRESSION MODEL

3.1 Introduction

After looking at various regression approaches, we opt for multi-order polynomial models. We followed a standard fitting approach to optimise scaling factors. Past this optimisation, we could simulate design spectra through Eq. (12). This equation reflects the prominence of the varying $\overline{U}_{max,r}$ and natural frequency, while taking into account the influence of all other controlling variables through sub-regression models (scale factors), f_s.

$$\widehat{S_a} = f(T, \overline{U}_{max,r}) \cdot f_s(T, W) \cdot f_s(T, L/W) \cdot f_s(T, H/W) \cdot f_s(T, \xi) \cdot f_s(T, z_{\overline{U}_{peak}}/H) \cdot$$
$$f_s(T, terrain) \cdot f_s(T, \psi) \cdot f_s(T, m_v) \cdot f_s(T, c_d) \tag{12}$$

Note in this equation the change to non-dimensional variables such as chord to width (L/W), height to width (H/W) and $z_{\overline{U}_{peak}}/H$ ratio which modifies Eq. (11) as in Eq. (13).

$$S_a = f(\overline{U}_{max,r}, W, L/W, H/W, z_{\overline{U}_{peak}}/H, \xi, m_v, c_D, terrain, \psi) \tag{13}$$

Furthermore, the non-linear relationship of the TWDS, T and $\bar{U}_{max,r}$ define a three-dimensional surface as shown in Fig. 2, abstracted in the three-order polynomial regression model given by Eq. (14).

$$\widehat{S_{a,u}} = b_1 + b_2\bar{U}_{max,r} + b_3T + b_4\bar{U}_{max,r}^2 + b_5T^2 + b_6T\bar{U}_{max,r} + b_7\bar{U}_{max,r}^3 + b_8\bar{U}_{max,r}^2T + b_9\bar{U}_{max,r}T^2 + b_{10}T^3 \tag{14}$$

In this equation, $T = T + \Delta T_0$ and $\bar{U}_{max,r} = \bar{U}_{max,r} + \Delta\bar{U}_{max,r,0}$. The unknown parameters b_j were adjusted to minimise the difference between the TWDS and non-linear regression model (NLRM). That difference was estimated with $\min\limits_{b_{j,p}}\sum_{i=1}^{n}(\frac{\widehat{S_{a,i}}-S_{a,i}}{S_{a,i}})^2$, where n is the number of data points, i is an index for the current TWDS values, j represents the index of the unknown series of scaling factor and p represents the random input parameters (i.e., $\bar{U}_{max}$ in this case). The mean square error of the proposed model is, therefore, $\frac{1}{n}\sum_{i=1}^{n}(\widehat{S_{a,i}} - S_{a,i})^2$.
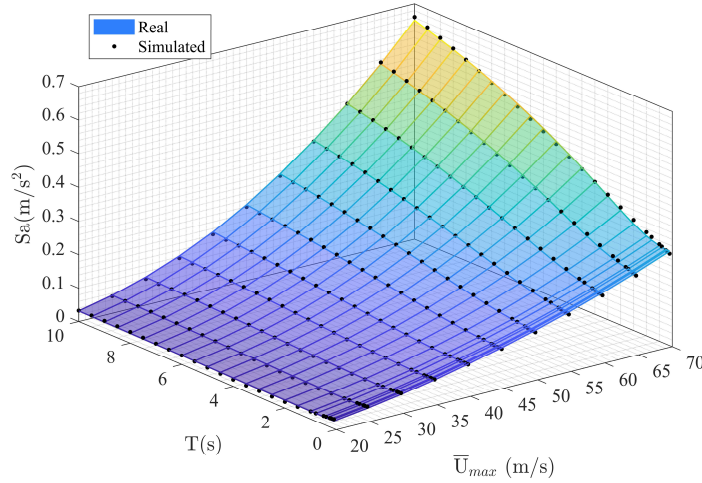
Fig. 2. Comparison between the real and simulated values of TWDS with varying T and $\bar{U}_{max}$.

It follows that differences in spectral ordinates with other controlling parameters could also be determined through separate polynomial regression modelling, which brings in the relationship $S_{a,P}\big/S_{a,P_d}$ - where P_d is a randomly selected controlling parameter. Eq. (15) provides such mathematical definition.

$$\widehat{S_{a,P}}\big/\widehat{S_{a,P_d}} = b_{1,P} + b_{2,P}P + b_{3,P}T + b_{4,P}P^2 + b_{5,P}T^2 + b_{6,P}TP + b_{7,P}P^3 + b_{8,P}P^2T + b_{9,P}PT^2 + b_{10,P}T^3 \tag{15}$$

With this in hand, the TWDS can be finally obtained with Eq. (16).

$$\widehat{S_a} = S_{a,\overline{U}_{max}} \times \left(\widehat{S_{a,W}}/\widehat{S_{a,W_d}}\right) \times \left(\widehat{S_{a,L/W}}/\widehat{S_{a,(L/W)_d}}\right) \times \left(\widehat{S_{a,H/W}}/\widehat{S_{a,(H/W)_d}}\right) \times \left(\widehat{S_{a,\xi}}/\widehat{S_{a,\xi_d}}\right) \times$$
$$\left(S_{a,z_{\overline{U}_{peak}}}/S_{a,(z_{\overline{U}_{peak}})_d}\right) \times \left(\widehat{S_{a,\psi}}/\widehat{S_{a,\psi_d}}\right) \times \left(\widehat{S_{a,m_v}}/\widehat{S_{a,(m_v)_d}}\right) \times \left(\widehat{S_{a,c_d}}/\widehat{S_{a,(c_d)_d}}\right) \times$$
$$\left(S_{a,terrain}/S_{a,(terrain)_d}\right) \tag{16}$$

In this context, we could always infer the variation of the main polynomial regression model with respect to any controlling parameter. Eq. (17) illustrates by using the width of the building.

$$\widehat{S_{a,W}}\Big/\widehat{S_{a,W_d}} = b_{1,W} + b_{2,W}W + b_{3,W}T + b_{4,W}W^2 + b_{5,W}T^2 + b_{6,W}TW + b_{7,W}W^3 +$$
$$b_{8,W}W^2T + b_{9,W}WT^2 + b_{10,W}T^3 \tag{17}$$

Table 2 lists the optimised scaling factors used to fit the three-dimensional NLRM of the TWDS and normalised TWDS. In this case, the root mean square error (RMSE) between the simulated and real TWDS with varying velocity is 0.0036 (see - Fig. 2).

Table 2. Scaling factors for three-dimensional NLRM of the TWDS and normalised TWDS.

Inputs, P	TWDS $S_{a,\overline{U}_{max}}$	Normalised TWDS ($\widehat{S_{a,P}}\big/\widehat{S_{a,P_d}}$)								
	$\overline{U}_{max}$ (m/s)	W (m)	L/W	H/W	ξ	$z_{\overline{U}_{peak}}/H$	Terrain	ψ	m_v (kg/m^3)	c_d
Initials	25	20	1	10	0.025	50	B	1.5	384	1
$b_{1,P}$	-0.0044	8.6196	6.8902	2.4571	1.0110	-0.4401	1.6860	0.7397	6.4135	0.0000
$b_{2,p}$	0.0013	-1.1379	-18.3407	-1.7015	-0.8597	7.6957	-0.1931	0.3502	-0.0383	1.0000
$b_{3,P}$	-0.0084	0.4278	0.0016	0.5236	0.0240	-0.0278	0.0001	0.0145	0.0004	-0.0000
$b_{4,P}$	0.0000	0.0691	24.3069	0.6987	9.9217	-9.1043	-0.1227	-0.1594	0.0001	-0.0000
$b_{5,P}$	0.0027	0.0257	-0.0005	0.0333	-0.0046	0.0031	-0.0000	-0.0000	-0.0000	0.0000
$b_{6,p}$	-0.0003	-0.0578	-0.0021	-0.3223	-0.4193	0.1001	-0.0000	-0.0157	-0.0000	0.0000
$b_{7,p}$	0.0000	0.0000	-17.0451	-0.1304	-26.8763	3.7998	0.0239	0.0279	-0.0000	0.0000
$b_{8,p}$	0.0000	0.0025	0.0010	0.0578	1.1876	-0.0246	0.0000	0.0035	0.0000	-0.0000
$b_{9,P}$	0.0000	0.0001	0.0004	0.0201	-0.0037	-0.0032	0.0000	0.0002	0.0000	-0.0000
$b_{10,P}$	-0.0001	-0.0058	0.0001	-0.0160	0.0003	-0.0002	0.0000	-0.0000	0.0000	-0.0000
RMSE	0.0036	0.0141	0.0042	0.0265	0.0303	0.0134	0.0000	0.0005	0.0078	0.0000

3.2 Validation of non-linear regression model

Fig. 3 shows how the real and simulated TWDS (NLRM), compare. The RMSE between real and simulated TWDS values is shown in Table 3 to Table 5.
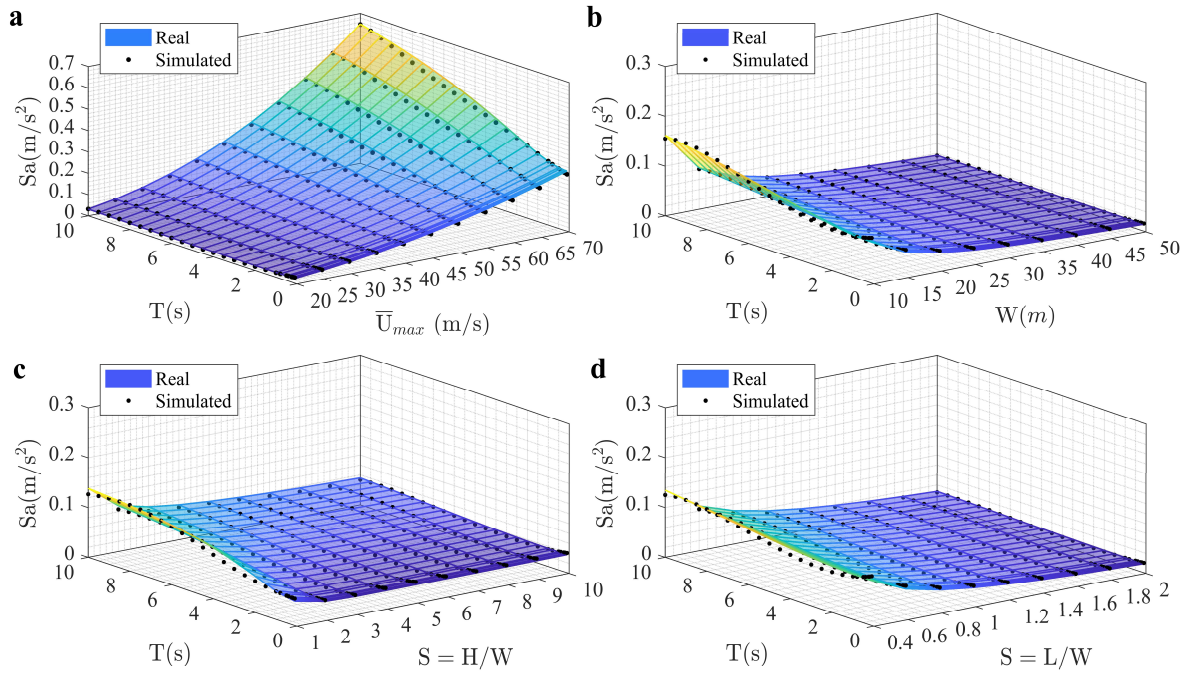
Fig. 3. Comparison between the real and simulated TWDS considering local variations of input parameters: (a) $\overline{U}_{max}$; (b) W; (c) H/W; (d) L/W.

The maximum error (14.36%) estimated for these results occurs when the velocity is at 20 m/s. Note that the error parameter remains below 7.6% when the velocity equals or exceeds 25 m/s. The maximum error ratios of the simulated TWDS with varying W, H/W and L/W equal 8.29%, 8.18% and 8.02%, respectively.

Table 3. RMSE for varying parameters.

$\overline{U}_{max,r}$ (m/s)	$\sqrt{\overline{e^2}}$	$\overline{S_a}$	$\sqrt{\overline{e^2}}/\overline{S_a}$	W (m)	$\sqrt{\overline{e^2}}$	$\overline{S_a}$	$\sqrt{\overline{e^2}}/\overline{S_a}$	H/W	$\sqrt{\overline{e^2}}$	$\overline{S_a}$	$\sqrt{\overline{e^2}}/\overline{S_a}$
20	0.0037	0.0258	0.1436	10	0.0077	0.1144	0.0671	1	0.0078	0.0950	0.0818
25	0.0032	0.0421	0.0760	15	0.0040	0.0622	0.0638	2	0.0032	0.0615	0.0516
30	0.0032	0.0632	0.0509	20	0.0032	0.0421	0.0760	3	0.0042	0.0526	0.0806
35	0.0037	0.0896	0.0418	25	0.0023	0.0318	0.0721	4	0.0037	0.0485	0.0754
40	0.0048	0.1216	0.0393	30	0.0018	0.0255	0.0718	5	0.0033	0.0461	0.0717
45	0.0063	0.1594	0.0394	35	0.0015	0.0214	0.0712	6	0.0033	0.0446	0.0730
50	0.0082	0.2034	0.0405	40	0.0014	0.0185	0.0743	7	0.0035	0.0436	0.0793
55	0.0107	0.2537	0.0421	45	0.0011	0.0163	0.0656	8	0.0034	0.0429	0.0784
60	0.0137	0.3106	0.0440	50	0.0012	0.0146	0.0829	9	0.0028	0.0424	0.0672
65	0.0172	0.3743	0.0460					10	0.0032	0.0421	0.0760
70	0.0215	0.4449	0.0483								

$\overline{S_a}$ is the mean value of the real TWDS of the output acceleration with varying T (natural period).

The maximum error (19.74%) with varying damping ratio occurs when this parameter is 0.01. With the increasing of the damping ratio, the RMSE floats at 8%. The errors estimated with varying modal shape factor (φ), the structural mass per unit volume (m_v), terrain and the ratio of the $z_{\bar{U}_{peak}}/H$ are less than 8.43%.

Table 4. RMSE for varying parameters

L/W	$\sqrt{\overline{e^2}}$	$\overline{S_a}$	$\sqrt{\overline{e^2}}/\overline{S_a}$	ξ	$\sqrt{\overline{e^2}}$	$\overline{S_a}$	$\sqrt{\overline{e^2}}/\overline{S_a}$	φ	$\sqrt{\overline{e^2}}$	$\overline{S_a}$	$\sqrt{\overline{e^2}}/\overline{S_a}$
0.4	0.0081	0.1052	0.0768	0.01	0.0097	0.0493	0.1974	0.8	0.0030	0.0400	0.0751
0.6	0.0053	0.0701	0.0752	0.025	0.0032	0.0421	0.0760	0.9	0.0030	0.0405	0.0752
0.8	0.0042	0.0526	0.0794	0.05	0.0030	0.0392	0.0767	1.0	0.0031	0.0408	0.0753
1.0	0.0032	0.0421	0.0760	0.1	0.0031	0.0376	0.0823	1.1	0.0031	0.0412	0.0754
1.2	0.0026	0.0351	0.0740	0.2	0.0031	0.0368	0.0840	1.2	0.0031	0.0414	0.0755
1.4	0.0023	0.0301	0.0775	0.25	0.0030	0.0366	0.0821	1.3	0.0032	0.0417	0.0757
1.6	0.0021	0.0263	0.0802					1.4	0.0032	0.0419	0.0758
1.8	0.0017	0.0234	0.0735					1.5	0.0032	0.0421	0.0760
2.0	0.0016	0.0210	0.0775					1.6	0.0032	0.0423	0.0760

Table 5. RMSE for varying parameters

m_v (kgm^{-3})	$\sqrt{\overline{e^2}}$	$\overline{S_a}$	$\sqrt{\overline{e^2}}/\overline{S_a}$	$Terr.$	$\sqrt{\overline{e^2}}$	$\overline{S_a}$	$\sqrt{\overline{e^2}}/\overline{S_a}$	$z_{\bar{U}_{peak}}/H$	$\bar{e}^2$	$\overline{S_a}$	$\sqrt{\overline{e^2}}/\overline{S_a}$
150	0.0085	0.1077	0.0789	B	0.0032	0.0421	0.0760	0.125	0.0012	0.0147	0.0843
200	0.0061	0.0808	0.0752	C	0.0021	0.0272	0.0760	0.250	0.0032	0.0421	0.0760
250	0.0052	0.0646	0.0811	D	0.0015	0.0201	0.0760	0.375	0.0042	0.0596	0.0703
300	0.0043	0.0539	0.0805					0.5	0.0048	0.0704	0.0678
350	0.0034	0.0462	0.0747					0.625	0.0053	0.0776	0.0686
384	0.0032	0.0421	0.0760					0.75	0.0060	0.0827	0.0722
400	0.0033	0.0404	0.0815					1	0.0060	0.0894	0.0674

Finally, Fig. 4 illustrates differences obtained for 6 different scenarios. The RMSE for these six cases are 0.0032, 0.0244, 0.0113, 0.0118, 0.0349 and 0.0174, while the maximum error does not exceed 3.5%.
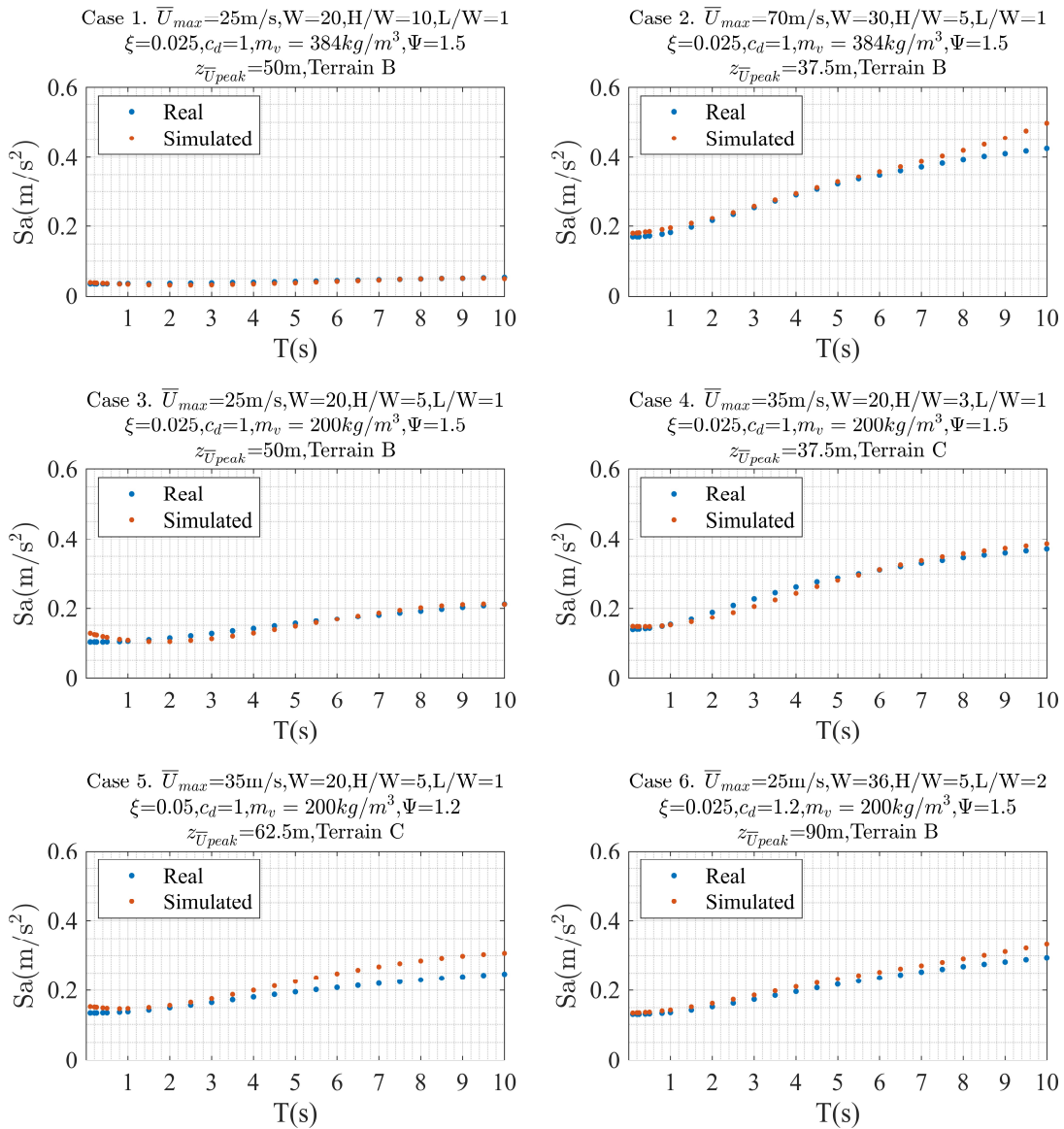
Fig. 4. Comparison of real and simulated design spectra for scenarios.

4. DYNAMIC RESPONSE OF CAARC TALL BUILDING

4.1 Description of the structure

The Commonwealth Advisory Aeronautical Research Council (CAARC) benchmark building (Melbourne, 1980) is utilized in this section for checking the accuracy of structural vibrations obtained with real and synthetic design spectra. This building dimensions are 46 m width (W) × 30 m chord (L) × 183 m height (H), as shown in Fig. 5 (a). The natural frequency of the building is 0.2 Hz along the x and y directions. The fraction of the critical damping equals 0.01 and the mass per unit volume of the building is assumed to be 160 kg/m^3.
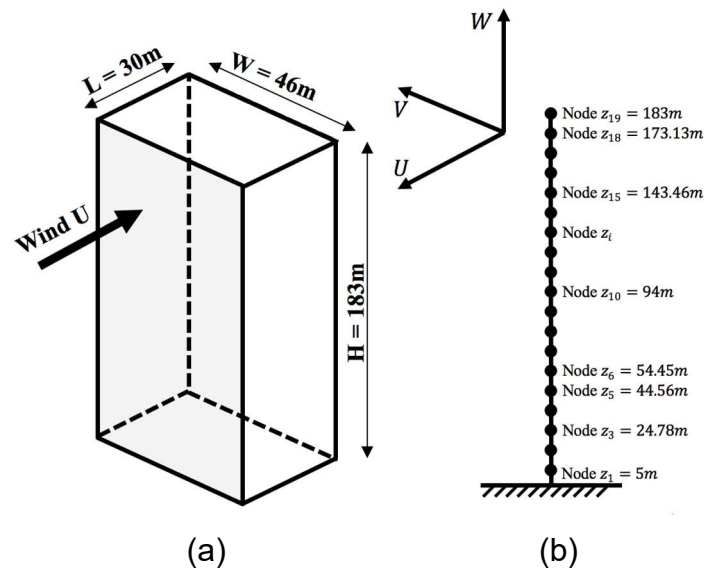
Fig. 5. The CAARC benchmark building, (a) The dimensions; (b) The simplified modelling.

The building was modelled as a vertical mast formed by 19 members and 19 joints, as shown in Fig. 5 (b). The MDOF system was discretised into a 3D grid conformed with lumped masses. The interstorey at the basement is 5 m and is around 9.89 m for the remaining levels. The width of the building was equally divided into 5 bays and enclosed within 6 nodes, whereas the distance between each pair of adjacent nodes is 9.2 m. The chord of the building was equally divided into 3 bays enclosed within 10 m for adjacent modes.

4.2 Validation of the simulated model

The benchmark building went into a standard modal analysis using the simulated TWDS. The peak displacement response can be obtained by the sum of the static displacement and the *rms* of the dynamic displacement. The real and simulated dynamic displacements at the top of the building are shown in Table 6. The analysis considered two scenarios: (a) horizontal and vertical wind fluctuations, and (b) wind gusts partially correlated in the vertical direction only. This results in a peak displacement at the top of the building of 0.328 m and 0.351 m for scenarios (a) and (b), respectively. The equivalent displacements obtained when using synthetic design spectra are respectively 0.328 m and 0.341 m. This yields differences of 0% and 9.7%, being the most accurate simulation, whose real spectra have taken into consideration of the horizontal and vertical gust correlation. These results are also illustrated in Fig. 6, where d_x and d_y represent the lateral displacement amplitudes at different heights in x and y direction separately.

Table 6. Lateral displacements at the top of the building.

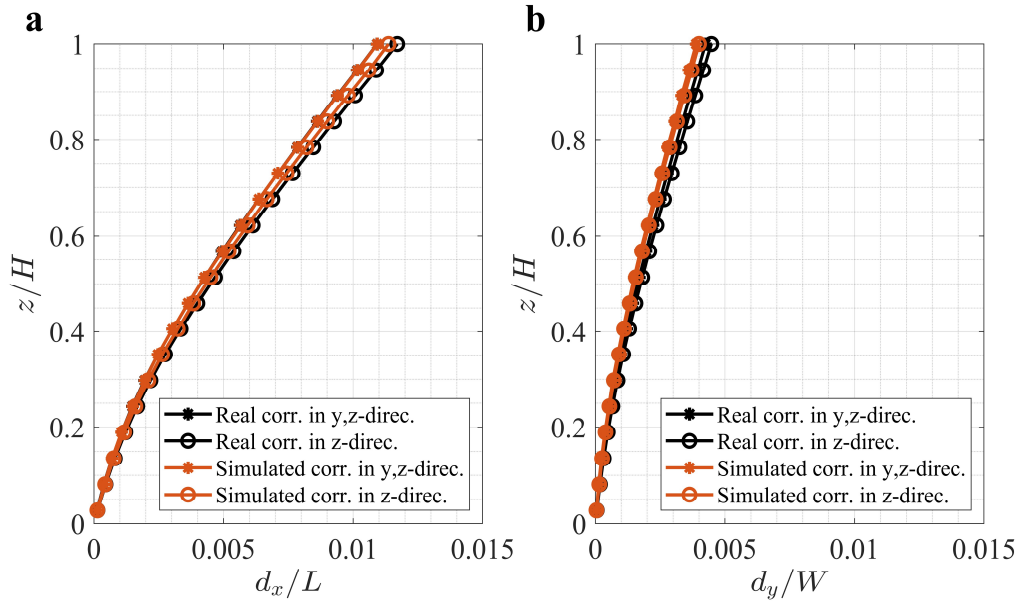| Direction	$\bar{U}_H$ (ms^{-1})	Static $\Delta = f_1/k_1$	Davenport's coherence (vertical and horizontal)				Partial correlated (vertical only)			
			Real Dyna.	Simu. Dyna.	Real Total	Simu. Total	Real Dyna.	Simu. Dyna.	Real Total	Simu. Total
x	32.06	0.200	0.128	0.128	0.328	0.328	0.151	0.141	0.351	0.341
y	32.06	0.112	0.084	0.067	0.196	0.179	0.094	0.072	0.206	0.184

Fig. 6. Reduced lateral displacements with varying heights, (a) In x-direction; (b) In y-direction.

5. CONCLUSION

This paper shows how recently developed thunderstorm downburst wind design spectra with random input variables can be generalised through a non-linear regression model. This regression approach assembles the controlling input parameters to form one polynomial equation which largely simplifies the derivation of design spectra, which otherwise had to be done on a one-by-one basis i.e. taking into account mechanical and aerodynamical properties of buildings. The accuracy of the regression modelling was validated through various scenarios whereby controlling parameters varied randomly. This results in an estimated RMSE relating real and simulated spectra below 3.5%. The investigation highlighted that the varying maximum running mean velocity observed during thunderstorms has a strong impact on the amplitude of design spectral ordinates with lower influence on various other controlling parameters.

Real and synthetic design spectra were then used to run a standard model analysis, to verify the accuracy of the overall approach. The dynamic analysis used a benchmark building with regular geometry and uniform mass distribution, which reported differences below 10% related to peak dynamic displacements.

This suggests that the synthetic wind design spectra could offer an alternative for designers to quickly calculate the dynamic response on structures.

REFERENCES

Asano, K., Iida, Y., & Uematsu, Y. (2019). Laboratory study of wind loads on a low-rise building in a downburst using a moving pulsed jet simulator and their comparison with other types of simulators. Journal of wind engineering and industrial aerodynamics, 184, 313-320.

Chen, L., & Letchford, C. (2004). A deterministic–stochastic hybrid model of downbursts and its impact on a cantilevered structure. Engineering Structures, 26(5), 619-629.

Davenport, A. (1977). The prediction of the response of structures to gusty wind. Safety of structures under dynamic loading, 1, 257-284.

Dyrbye, C., & Hansen, S. O. (1997). Wind loads on structures.

Haines, M., & Taylor, I. (2018). Numerical investigation of the flow field around low rise buildings due to a downburst event using large eddy simulation. Journal of wind engineering and industrial aerodynamics, 172, 12-30.

Jesson, M., Sterling, M., Letchford, C., & Baker, C. (2015). Aerodynamic forces on the roofs of low-, mid- and high-rise buildings subject to transient winds. Journal of wind engineering and industrial aerodynamics, 143, 42-49.

Jesson, M., Sterling, M., Letchford, C., & Haines, M. (2015). Aerodynamic forces on generic buildings subject to transient, downburst-type winds. Journal of wind engineering and industrial aerodynamics, 137, 58-68.

Kareem, A., Hu, L., Guo, Y., & Kwon, D.-K. (2019). Generalized wind loading chain: Time-frequency modeling framework for nonstationary wind effects on structures. Journal of Structural Engineering, 145(10), 04019092.

Le, T.-H., & Caracoglia, L. (2017). Computer-based model for the transient dynamics of a tall building during digitally simulated Andrews AFB thunderstorm. Computers & Structures, 193, 44-72.

Lombardo, F. T., Mason, M. S., & de Alba, A. Z. (2018). Investigation of a downburst loading event on a full-scale low-rise building. Journal of wind engineering and industrial aerodynamics, 182, 272-285.

Melbourne, W. (1980). Comparison of measurements on the CAARC standard tall building model in simulated model wind flows. Journal of wind engineering and industrial aerodynamics, 6(1-2), 73-88.

Peng, L., Huang, G., Chen, X., & Yang, Q. (2018). Evolutionary spectra-based time-varying coherence function and application in structural response analysis to downburst winds. Journal of Structural Engineering, 144(7), 04018078.

Solari, G. (2016). Thunderstorm response spectrum technique: theory and applications. Engineering Structures, 108, 28-46.

Solari, G. (2020). Thunderstorm downbursts and wind loading of structures: Progress and prospect. Frontiers in built environment, 6, 63.

Solari, G., Rainisio, D., & De Gaetano, P. (2017). Hybrid simulation of thunderstorm outflows and wind-excited response of structures. Meccanica, 52(13), 3197-3220.

Song, J., Martinez-Vazquez, P., & Skalomenos, K. A. (2021). A framework on the dynamic response of tall structures to non-stationary wind using design spectrum. 8th ECCOMAS Thematic Conference on Computational Methods in Structural Dynamics and Earthquake Engineering, Athens, Greece.